

Non-magnetic negative-refraction systems for terahertz and far-infrared frequencies

Leonid V. Alekseyev¹, Viktor A. Podolskiy² and Evgenii E. Narimanov¹

¹ *Electrical and Computer Engineering Department, Purdue University, West Lafayette, IN 47907*

² *Physics Department, University of Massachusetts, Lowell, MA 01854*

Compiled November 25, 2021

We demonstrate that homogeneous naturally-occurring materials can form non-magnetic negative refractive index systems, and present specific realizations of the proposed approach for the THz and far-IR frequencies. The proposed structure operates away from resonance, thereby promising the capacity for low-loss devices. © 2021 Optical Society of America

Following the initial proposal by Veselago in 1968,¹ negative refraction materials spent over 30 years as a forlorn curiosity before being resurrected with renewed interest from both theoretical and experimental groups. Within the last several years it was realized that these materials (known also as left-handed materials) possess unusual properties, some of which were not recognized at the time of their conceptions. These properties include resonant enhancement of evanescent fields, potentially enabling near-perfect imaging below the diffraction limit and leading to a new class of optical devices,² as well as nontrivial behavior in the nonlinear regime.³ Despite initial controversy over the realizability of negative index materials (NIMs), successful proof of principle demonstrations have been accomplished.^{4,2,5,6,7}

Existing designs for left-handed materials rely on achieving overlapping dipolar and magnetic resonances,^{8,9} or using photonic crystals near the bandgap.^{10,2} Both of these approaches necessitate complicated 3D patterning of the medium with microstructured periodic arrays. Fabrication of such structures presents significant challenges even for GHz applications, while manufacturing systems for higher frequencies becomes harder still. Furthermore, near-resonant operational losses impose severe limitations on the imaging resolution.²²

As an alternative to periodic systems, a waveguide-based implementation of a NIM was proposed,¹¹ which obviates the need for negative magnetic permeability and does not require periodic patterning. This approach circumvents major manufacturing obstacles to achieving NIM behavior at terahertz or optical frequencies.

To achieve this behavior, the waveguide material must possess characteristics of a uniaxial medium with a significant anisotropy. Furthermore, this anisotropy must ensure that ϵ_{\perp} (the component of ϵ transverse to the planar waveguide) is negative, while ϵ_{\parallel} (in-plane component) remains positive. TM modes in such waveguide undergo negative refraction in the waveguide plane, and propagate with negative phase velocity.¹¹

One of the key aspects in designing such an NIM system is selecting the material for the waveguide's anisotropic core. Several options have been proposed for

the core material, in particular, nanostructured composites in a dielectric host and quantum well structures.¹¹ While being within the grasp of existing technology, the fabrication of such systems remains highly challenging.

In this Letter we present an alternative approach to non-magnetic NIMs for THz and far-infrared domains based on naturally occurring materials with large dielectric anisotropy. In particular, we discuss the possibility of negative refraction in a waveguide-based system at approximately 20 μm , 58 μm and 255 μm using, respectively, sapphire, bismuth, or triglycine sulfate in the waveguide core. We focus on monocrystalline bismuth as an attractive option for manufacturing the NIM waveguide core thanks to its large anisotropy and availability of samples with high purity.

In a planar waveguide with anisotropic dielectric core the wave vector components k_z and k_y are governed by the dispersion relation

$$k_z^2 + k_y^2 = \epsilon \nu \frac{\omega^2}{c^2}, \quad (1)$$

with $\nu = (1 - \kappa^2 c^2 / \epsilon_{\parallel} \omega^2)$ where ω is the frequency of light, $\epsilon = \epsilon_{\perp}(\epsilon_{\parallel})$ for the TM(TE) modes, κ is the transverse mode parameter, and k_z and k_y lie in the waveguide plane. For perfectly conducting waveguide walls (a good approximation for silver and other metals at THz and far-IR frequencies¹²), $\kappa = m\pi/d$, where m is an integer and d is the thickness of the waveguide.¹¹ The effective refractive index for propagating waveguide modes in this system is given by $n_{\text{eff}}^2 = \epsilon \nu$. To support propagating modes, ϵ and ν must have the same sign. The case $\epsilon > 0$, $\nu > 0$ is typically realized in an isotropic planar waveguide operating above cut-off. However, in the case $\epsilon < 0$, $\nu < 0$ negative refraction occurs,¹¹ with refractive index given by

$$n_{\text{eff}} = -\sqrt{\epsilon_{\perp} \nu}. \quad (2)$$

Note that if κ is regarded as the transverse wave vector component, Eq.(1) can be rewritten as a hyperbolic dispersion relation $k_{\perp}^2/\epsilon_{\parallel} - k_{\parallel}^2/|\epsilon_{\perp}| = \omega^2/c^2$, identified in Ref. [13] with the onset of negative refraction.

As follows from the definition of ν , the propagation with negative phase velocity occurs only for TM modes

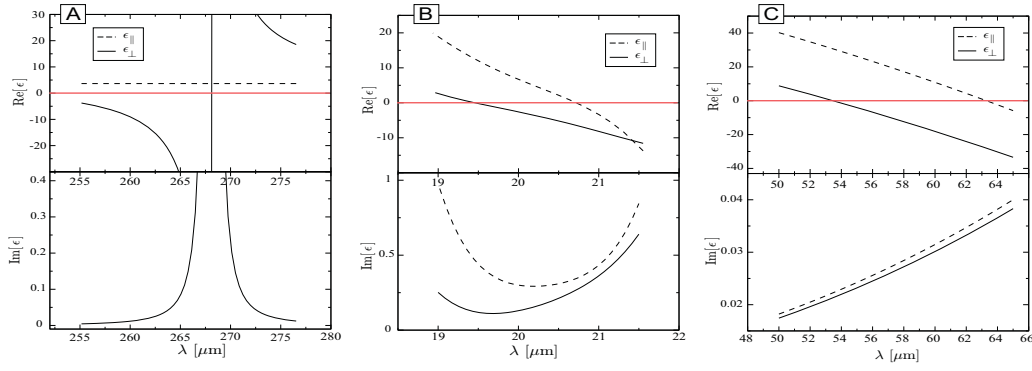


Fig. 1. (A): The real (top panel) and the imaginary (bottom panel) parts of the dielectric function of TGS; the monoclinic C_2 axis is along the “perpendicular” (\perp) direction. (B): Same for sapphire; the crystallographic c axis is along the “perpendicular” (\perp) direction. (C): Same for monocrystalline bismuth.

when $\epsilon_{\parallel} > 0$, $\epsilon_{\perp} < 0$. This behavior is observed in a number of materials where structural anisotropy strongly affects the dielectric response.

One example of such materials is triglycine sulfate (TGS), a compound widely used in fabricating infrared photodetectors. Spectroscopic studies of the crystal at low temperature have shown that phonon modes polarized parallel to the crystal’s monoclinic C_2 axis significantly differ in frequency from phonons transverse to the axis. This results in a large anisotropy in the dielectric tensor along these directions. In particular, dielectric response for the field polarized *along* the C_2 axis features a resonance at $268 \mu\text{m}$, which is absent if the incident field is polarized *transverse* to the C_2 axis.¹⁴ Dielectric function ϵ_{\perp} in the vicinity of this resonance can be fitted with the Lorentz-Drude model,¹⁵ while ϵ_{\perp} in this region can be taken approximately constant.^{14,16} Lorentz-Drude model parameters from Ref. [15] were used to construct Fig. 1(a). As is evident from the figure, $\epsilon_{\perp} < 0$, while $\epsilon_{\parallel} > 0$ in the region $250 \leq \lambda \leq 268 \mu\text{m}$. Furthermore, the imaginary part of ϵ becomes small away from the resonance, minimizing absorption. A TGS-filled waveguide with C_2 axis oriented perpendicular to the waveguide plane would support negative index propagation, while suffering from minimal propagation losses ($\text{Im}[\epsilon] \sim 10^{-3}$ at $250 \mu\text{m}$).

Whereas the phonon anisotropy of TGS exists in the low-THz domain, for other materials, it may occur in a different spectral band. In particular, the strong anisotropy of the dielectric response of sapphire (Al_2O_3) is also due to excitation of different phonon modes (polarized either parallel or perpendicular to the c axis of the rhombohedral structure), but occurs around $20 \mu\text{m}$. Fig. 1(b) shows experimentally-determined¹⁷ ϵ_{\parallel} and ϵ_{\perp} as functions of frequency. As with TGS, a region of $\epsilon_{\perp} < 0$, $\epsilon_{\parallel} > 0$ is evident in the experimental data. This potentially enables a sapphire-based waveguide NIM (with the c axis of sapphire core perpendicular to the waveguide plane). Note that the minimum of the material absorption occurs in the frequency range of interest.

Anisotropic phonon excitations are not the only mechanism that can lead to strong dielectric anisotropy. Bismuth, a Group V semimetal with rhombohedral lattice and trigonal symmetry, exhibits such anisotropy due to a substantial difference in its electron effective masses along different directions in the crystal.

In the frequency region of interest, the spectral dependence of the electric permittivity of Bismuth can be adequately described by the Drude model,

$$\epsilon = \epsilon_L \left(1 - \frac{\omega_{\text{pl}}^2}{\omega^2 + i\omega\tau^{-1}} \right), \quad (3)$$

with ϵ_L the lattice permittivity, $\omega_{\text{pl}} = Ne^2/\epsilon_L m_{\text{eff}}$ the plasma frequency, and τ the relaxation time. These parameters are known from interferometric and reflectance studies of Bi samples. In particular, plasma frequency of pure Bismuth at 4 K was measured to be 158 cm^{-1} for the incident E -field polarized perpendicular to the trigonal axis, and 186 cm^{-1} for the field polarized parallel to the axis.¹⁸ These values are in agreement with other experiments.^{19,20} The lattice dielectric constant ϵ_L for the field perpendicular to the trigonal axis was found to be 110 ± 10 ,²⁰ in reasonable agreement with Ref. 19. For polarization parallel to the trigonal axis, $\epsilon_L = 76$.²¹

There can be substantial variation in the relaxation time τ depending on the purity of the sample. We take $\tau = 0.1 \text{ ns}$,²⁰ however, this is a conservative estimate; for low temperatures, relaxation times over an order of magnitude greater have been reported as far back as 1975.²¹ Even with $\tau = 0.1 \text{ ns}$, the typical ratio of imaginary and real parts of the dielectric function in Bi is on the order of 0.1% in the frequency interval of interest, which enables many imaging and transmission applications.²² It should also be noted that high-quality single-crystal films as thin as $1 \mu\text{m}$, with the trigonal axis (C_3) oriented perpendicular to the film plane, have been reported,²³ thereby essentially solving the technological issues in fabricating the proposed negative index device.

Fig. 1(c) shows the behavior of real and imaginary

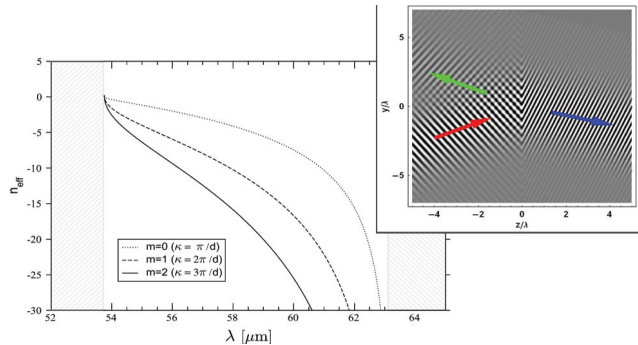


Fig. 2. The effective refractive index of the three lowest order modes in a bismuth waveguide. Inset: numerical simulation showing the refraction of a beam within a metallic waveguide (of thickness $d = 4.5 \mu\text{m}$) at an interface between an isotropic dielectric with $\epsilon = 55$ and monocrystalline bismuth; $\lambda = 61 \mu\text{m}$.

components of ϵ for Bi based on Eq.(3). The most prominent feature of these plots, the transition from $\epsilon > 0$ to $\epsilon < 0$, is determined by the highly anisotropic plasma frequency. This anisotropy creates a window between $\lambda = 53.7 \mu\text{m}$ and $63.2 \mu\text{m}$ where $\epsilon < 0$ for the E -field along the C_3 axis, while $\epsilon > 0$ for E transverse to C_3 . The existence of such $10 \mu\text{m}$ window was confirmed by direct measurement.²⁴

To allow for left-handed propagation in this frequency interval, Bi should be integrated into the core of a planar waveguide, with the C_3 axis oriented in the transverse direction. In Fig. 2 we examine the behavior of the effective refractive index n_{eff} [Eq.(2)] for the proposed subcritical ($d < \lambda/2$) waveguide structure with bismuth core. Note that negative effective index is possible for all modes over the entire ($\epsilon_{\perp} < 0$, $\epsilon_{\parallel} > 0$) range. Negative refraction behavior of our system was further confirmed by a numerical calculation of the electric field incident on the Bi waveguide. The results of this calculation are presented in Fig. 2 (inset). We assume a TM wave with a gaussian profile, mode-matched into the Bi waveguide in the transverse direction by e.g. propagating the beam from a metallic waveguide of the same thickness, filled with a regular dielectric. One can clearly see the negative refraction at the boundary. Furthermore, it is evident that attenuation of the transmitted wave is weak, as expected from low values of the imaginary part of the dielectric constant [Fig. 1(c)].

In addition, this calculation shows that the NIM waveguide remains transparent despite the fact that transverse dimension of the waveguide is much smaller than the wavelength, which indicates strong confinement of the field within the core (since the cladding is assumed to be perfectly conducting). This behavior is not found in a subwavelength dielectric waveguide, where much of the field spreads into the cladding, or a subwavelength metallic waveguide, which does not support propagating modes. Such strong field confinement may find applica-

tions in photonic structures and nonlinear optics.²⁵

In conclusion, we have proposed a novel negative refraction system for several wavelengths from low-THz to far-IR. Our approach is non-magnetic, avoids the use of periodic patterning, utilizes naturally occurring materials, and promises the capacity for low-loss devices.

This work was partially supported by NSF grants DMR-0134736, ECS-0400615, the Princeton Institute for the Science and Technology of Materials (PRISM), GRF-OSU, and ACS-PRF.

References

1. V. G. Veselago, *Sov. Phys. Usp.* **10**, 509 (1968).
2. P. V. Parimi, W. T. Lu, P. Vodo, and S. Sridhar, *Nature* **426**, 404 (2003).
3. I. R. Gabitov, R. A. Indik, N. M. Litchinitser, A. I. Maimistov, V. M. Shalaev, and J. E. Soneson, *J. Opt. Soc. Am. B* **23**, 535 (2006).
4. R. A. Shelby, D. R. Smith, and S. Schultz, *Science* **292**, 77 (2001).
5. V. M. Shalaev, W. Cai, U. K. Chettiar, H.-K. Yuan, A. K. Sarychev, V. P. Drachev, and A. V. Kildishev, *Optics Letters* **30**, 3356 (2005).
6. E. Schonbrun, T. Yamashita, W. Park, and C. J. Summers, *Phys. Rev. B* **73**, 195117 (2006).
7. G. Dolling, C. Enkrich, M. Wegener, C. M. Soukoulis, and S. Linden, *Science* **312**, 892 (2006).
8. D. R. Smith, W. J. Padilla, D. C. Vier, S. C. Nemat-Nasser, and S. Shultz, *Phys. Rev. Lett.* **84**, 4184 (2000).
9. C. Parazzoli, R. Gregor, K. Li, *et al.*, *Phys. Rev. Lett.* **90**, 107401 (2003).
10. M. Notomi, *Phys. Rev. B* **62**, 1069610705 (2000).
11. V. A. Podolskiy and E. E. Narimanov, *Phys. Rev. B* **2005**, 201101(R) (71).
12. R. Wangberg, J. Elser, E. E. Narimanov, and V. A. Podolskiy, *J. Opt. Soc. Am. B.* **23**, 498 (2006).
13. C. Luo, S. G. Johnson, and J. D. Joannopoulos, *Phys. Rev. B* **65**, 201104(R) (2002).
14. A. Hadni and X. Gerbaux, *Ferroelectrics* **248**, 15 (2000).
15. X. Gerbaux, M. Tazawa, and A. Hadni, *Ferroelectrics* **215**, 47 (1998).
16. T. Dumelow, J. A. P. da Costa, and V. N. Freire, *Phys. Rev. B* **72**, 235115 (2005).
17. M. Schubert, T. E. Tiwald, and C. M. Herzinger, *Phys. Rev. B* **61**, 8187 (2000).
18. W. S. Boyle, A. D. Brailsford, and J. K. Galt, *Phys. Rev.* **109**, 1396 (1958).
19. W. S. Boyle and A. D. Brailsford, *Phys. Rev.* **120**, 1943 (1960).
20. V. D. Kulakovskii and V. D. Egorov, *Sov. Phys. Solid State* **15**(7), 1368 (1974).
21. V. S. Edelman, *Adv. Phys.* **25**, 555 (1976).
22. V. A. Podolskiy and E. E. Narimanov, *Opt. Lett.* **30**, 75 (2005).
23. F. Y. Yang, K. Liu, K. Hong, D. H. Reich, P. C. Searson, and C. L. Chien, *Science* **284**, 1335 (1999).
24. E. Gerlach, P. Grosse, M. Rautenberg, and W. Senske, *Phys. Stat. Sol. (b)* **75**, 553 (1976).
25. A. A. Govyadinov and V. A. Podolskiy, *Phys. Rev. B* **73**, 155108 (2006).